RSC Applied Polymers

PAPER

View Article Online
View Journal

Cite this: DOI: 10.1039/d6lp00058d

Redox-responsive photo-polymerizable PEG-based hydrogels: diverse functionalization, 3D-printing, and on-demand degradation for protein release

Meltem Alkis,†[a] Altan Gumuskaya,†[a] Salli Kocak,[a] Ismail Altinbasak,[a] Rana Sanyal[a,b] and Amitav Sanyal*[a,b]

Recent years have seen an ever-increasing utilization of redox-responsive polymeric materials for various biomedical applications. In this regard, the photopolymerization of poly(ethylene glycol) (PEG) polymers has been extensively explored for the fabrication of bulk and 3D-printed hydrogels, with applications in therapeutic and diagnostic uses. Herein, disulfide-containing PEG-based crosslinkers are obtained using a modular approach from commercially available linear PEGs and are used to produce redox-responsive bulk and 3D-printed gels that can encapsulate proteins and release them on demand under reducing conditions. Additionally, partial degradation of the disulfide linkages enables facile functionalization *via* thiol-maleimide and thiol-disulfide exchange chemistry, as demonstrated by reversible and irreversible attachment of fluorescent dyes. Furthermore, the obtained hydrogels and their degradation products exhibit high cytocompatibility, as evidenced by cytotoxicity and live/dead assays with cultured fibroblast cells. One can envision that this operationally simple approach to fabricating versatile redox-responsive hydrogels would enable its adaptation in various areas of biomedical sciences.

Received 16th February 2026,
Accepted 25th May 2026

DOI: 10.1039/d6lp00058d

rsc.li/rscapplpolym

Introduction

Polymeric materials are vital in enabling various biomedical applications since they can be designed and tailored to control their interaction with the biological world.[1–5] Such interaction could enable intricate communication of the polymeric scaffold with biological materials such as proteins and cells to augment their attachment and proliferation. On the other hand, protein and cell repellent surfaces are also in demand when anti-biofouling interfaces are needed, such as antibacterial coatings and sensor platforms.[6–12] In this context, hydrogels, a class of crosslinked soft materials that can absorb and hold water, have emerged as indispensable materials since they can be readily obtained from natural and synthetic polymers and can be engineered with diverse properties. In recent years, advances in synthetic polymer chemistry have enabled the fabrication of gels with varying physical and chemical properties, including facile post-gelation functionalization, further enhancing the functional attributes of these materials.[13–22] Apart from biocompatibility, tunable biodegradability plays an important role in various applications. In this regard, incorporation of stimuli-responsive dynamic linkages within hydrogels has emerged for biomedical applications ranging from delivery of drugs, proteins, and cells to tissue engineering.[23–25]

Over the past decade, a range of elegant chemical strategies have been developed to design stimuli-responsive hydrogels. While such advances are noteworthy, for eventual translation to a viable product, one of the most important aspects is the simplicity and scalability of the fabrication process. The hydrogel precursors should be readily available and involve straightforward chemical transformations, and the gelation process should be rapid and proceed with high efficiency under mild conditions. Although in recent years, since the advent of click chemistry, various novel approaches to hydrogel synthesis have been devised, simple photopolymerization continues to be a popular method of choice due to its operational simplicity, apart from high spatiotemporal control.[26]

Among the synthetic polymers as hydrogel precursors, poly(ethylene glycol) (PEG)-based materials are widely utilized due to their high biocompatibility and mechanical stability. Nonetheless, these PEG-based photo-polymerized hydrogels suffer from a lack of facile degradability, as well as poor cellular adhesion. Thus, approaches that impart stimuli-responsive

[a]*Department of Chemistry, Bogazici University, Bebek 34342, Istanbul, Türkiye. E-mail: amitav.sanyal@bogazici.edu.tr*
[b]*Bogazici University Center for Targeted Therapy Technologies, Bogazici University, 34684 Istanbul, Türkiye*
†These co-authors contributed equally.

degradation to PEG-based materials have been actively pursued over the past several years.[27,28] In particular, imparting PEG-based materials with redox-responsive degradation can expand their application in areas such as controlled release of drugs and biomolecules under benign and mild conditions. Redox-responsive linkages can be introduced as side-chain functional groups or along the backbone of the polymeric matrix, which allows the release of a conjugated or encapsulated functional molecule from the polymeric constructs.[29–34] Alternatively, the redox-responsive linkages are incorporated as crosslinkers, the disruption of which results in the degradation from the gel to the sol state. In the context of photopolymerization induced gelation, disulfide-containing crosslinkers, such as bis(2-methacryloyl)oxyethyl sulfide (DSDMA), a disulfide-based dimethacrylate, are among the most commonly employed redox-responsive linkers. Compared to the macromolecular PEG-based hydrogel precursors, small molecule based crosslinkers like this one would not only introduce tighter networks with limited swelling, but also pose challenges for obtaining 3D-printed structures using conventional extrusion-based printing techniques since it is a low molecular weight liquid. In this context, Matyjaszewski and co-workers reported the employment of a long-chain PEG crosslinker with a disulfide unit at the center.[35] Although an elegant approach, the utilization of hetero-telechelic PEG for making such a crosslinker makes the overall synthesis non-trivial. A more straightforward and modular approach to such redox-responsive crosslinkers would be desirable to fabricate redox-responsive hydrogels. Fabrication using photopolymerization provides spatial and temporal control over the fabrication process and thus expands the shapes, morphologies, and properties of the obtained materials. Furthermore, such redox-responsive photo-polymerizable hydrogels would also be attractive as bio-inks for printing hydrogel-based scaffolds that could undergo on-demand degradation in a stimuli-responsive fashion. Although some redox-responsive printed photo-polymerized hydrogels have been reported in recent years,[36,37] most reports, apart from some polyurethane-based elastomers and bio-based resins,[38,39] involve the incorporation of cleavable disulfide linkers to attach and release cargoes such as small molecules, peptides, and proteins rather than installing a redox-responsive degradation switch for the printed scaffold, as reported in this work.

Herein, we report the fabrication of PEG-based redox-responsive hydrogels using photopolymerization. To this end, a simple and scalable approach to obtain PEG-based macromolecular crosslinkers is developed. Commercially available linear PEG polymers are modified with methacrylate groups at the chain ends through a disulfide-based linker. Hydrogels with varying swelling and degradation properties can be obtained by the utilization of this redox-responsive crosslinker alone, or in conjunction with a non-degradable PEG-based crosslinker. Protein encapsulation and release under non-reducing and reducing conditions are demonstrated. Furthermore, it is shown that partial degradation of the disulfide linkers provides hydrogels that are amenable for non-reversible and reversible thiol-conjugation chemistries. Lastly, it is demonstrated that 3D-printed hydrogels that can undergo degradation in a redox-responsive manner can be obtained using the disulfide-containing PEG-based crosslinkers reported here.

Experimental

Materials

2-Hydroxyethyl methacrylate (HEMA) and 3,3′-dithiodipropionic acid (95%) were obtained from Sigma-Aldrich and used for synthesizing 2-[3-[(2-carboxyethyl)dithio]-1-oxopropoxy]ethyl 2-methyl-2-propenoate (HEMA-SS) which was obtained according to a previously reported procedure.[40] Poly(ethylene glycol) methyl ether methacrylate (PEGMEMA, M_n = 950 g mol^{-1}), poly(ethylene glycol) dimethacrylate (PEGDMA, M_n = 550 g mol^{-1}), and poly(ethylene glycol) (PEG, 4 kDa) were purchased from Sigma-Aldrich. Lithium phenyl-2,4,6-trimethylbenzoylphosphinate (LAP, 95%), 4-(dimethylamino)pyridine (DMAP, >99%), and 2,2′-dithiodipyridine were obtained from Sigma-Aldrich and then used as received. 1,4-Dithio-DL-threitol (DTT) was purchased from neoFroxx. *N*,*N*′-Dicyclohexylcarbodiimide (DCC) was obtained from Apollo Scientific. Gellan gum (G434) was purchased from PhytoTech Labs. SAMSA fluorescein, 5-((2-(and-3)-*S*-(acetylmercapto) succinoyl) amino) fluorescein, and mixed isomers (A685) were obtained from Thermo Fisher Scientific. Tetramethylrhodamine (TAMRA) maleimide, 5-isomer, was obtained from Lumiprobe. Fluorescein isothiocyanate conjugated bovine serum albumin (FITC-BSA) was purchased from Sigma. Anhydrous dichloromethane (DCM) and toluene were obtained from a SciMatCo purification system. Other solvents were obtained from Merck and used without further purification. Ultra-pure water was obtained *via* a Milli-Q Water Purification System (Merck Millipore, USA).

Characterization

FTIR spectra were recorded using a Thermo Scientific Nicolet 380 FT-IR spectrometer. ^{1}H NMR spectra were obtained using a Bruker Avance Ultrashield 400 (400 MHz) spectrometer. The molecular weights of the copolymers were determined by gel permeation chromatography (GPC) using a TSKgel Alpha-4000 column calibrated with poly(methyl methacrylate) (PMMA) standards using a refractive-index detector. 0.03% Lithium bromide in dimethylacetamide (DMAc) was used as an eluent at a flow rate of 1 mL min^{-1} at 30 °C. The morphology of the hydrogels was analyzed using a scanning electron microscope (SEM) (JEOL NeoScope JCM-500, with an accelerating voltage of 10 kV). The hydrogel samples were lyophilized and immersed in liquid nitrogen prior to SEM characterization. All rheological measurements of the hydrogels were performed using an ANTON PAAR MCR 302 rheometer. The release behaviors of FITC-BSA from the hydrogels were monitored *via* a UV/Vis spectrophotometer (Varian Cary 50 Scan). A Zeiss Z1 Observer inverted microscope with an Axiocam MRc5camera (ZEISS Fluorescence Microscopy, Carl Zeiss Canada Ltd,

Canada) was used for fluorescence images. Hydrogel precursor solutions were printed using an extruder-based 3D BIO X bioprinter (CELLINK, USA). One-way analysis of variance (ANOVA) within Tukey's *post hoc* tests was performed to determine statistical significance, which was accepted at a P value below 0.05 and generated using GraphPad Prism 10.6.1. All results, including mean values, were obtained from repeated measurements at least three times.

Synthesis of a methacrylate disulfide (MA-SS)-terminated telechelic PEG polymer (PEGDMASS)

HEMA-SS acid (0.33 g, 1.025 mmol) and PEG (4 kDa (M_n from the supplier), 1.02 g, 0.256 mmol) were dissolved in anhydrous DCM (3 mL), followed by stirring on ice. The solution of DCC (0.21 g, 1.025 mmol) and DMAP (0.06 g, 0.513 mmol) in 2 mL of anhydrous DCM was slowly added to the reaction mixture, and then allowed to stir at room temperature for 24 h. 5 mL of DCM was added to the mixture for dilution and then filtered to remove dicyclohexylurea (DCU). The solution was concentrated using rotary evaporation and then precipitated in isopropyl alcohol. The pure product was obtained with a yield of 79% (0.94 g). ^{1}H NMR ($CDCl_3$, δ, ppm), 6.13 (s, 2H, C═CH_2), 5.61 (s, 2H, C═CH_2), 4.36 (m, 4H, OCH_2CH_2), 4.27 (m, 4H, CH_2CH_2O), 3.85–3.42 (m, 370 H), 2.91 (t, 8H, SCH_2CH_2), 2.77 (t, 8H, $COCH_2CH_2$), 1.95 (s, 3H, CH_3C═CH_2).

Fabrication of hydrogels

A representative procedure for preparing hydrogels is described below. A deionized aqueous solution of a LAP initiator (0.5% wt/v) was sonicated for 30 min. An aqueous solution of a HEMA disulfide-terminated PEG polymer (PEGDMASS) (40 mg) and PEGMEMA (10 mg) was sonicated for 15 min. The control hydrogel groups contained PEGDMA (10 mg) for a 10% final concentration. Each solution was merged, vortexed and sonicated for 15 min to a final concentration of 10% w/v. 365 nm UV light exposure for 45 min yielded hydrogels. For loading of FITC-BSA, stock solutions (1 mg mL^{-1}) were freshly prepared. The final precursor solution contained 1% μg μL^{-1} of BSA. The obtained HGs were rinsed with water several times to remove any unreacted biomolecules or precursors. The swollen hydrogel sample was frozen and then freeze-dried *in vacuo* to yield the dried gel.

Swelling study

Dry hydrogel samples (W_0) were placed in 10 mL of distilled H_2O at room temperature. At regular intervals, the weight of the swollen hydrogel (W_t) was recorded after removing excess H_2O. The swelling ratio (W_{up}) was determined using eqn (1):

$$W_{up}\ (\%) = (W_t - W_0)/W_0 \times 100 \quad (1)$$

Rheological characterization

The rheological behavior of the swollen hydrogels was evaluated on an Anton Paar MCR 302 rheometer equipped with a 15 mm parallel plate geometry at room temperature. Oscillatory frequency (amplitude strain of 1%, 0.1–100 rad s^{-1}) and amplitude (angular frequency of 10 rad s^{-1}, 0.01–100% strain) sweep tests were performed using a Peltier temperature hood system. A 0.2 N axial force was applied to ensure tight contact between the samples and the plate. For stability and degradation measurements in different media (DI-H_2O/10 mM DTT), time sweep tests (amplitude strain of 1% and angular frequency of 10 rad s^{-1}) were performed at 37 °C using the Peltier temperature hood system to avoid medium evaporation. Oscillatory amplitude strain was varied from 1% to max% at 1 rad s^{-1} with 10 measuring points.

Protein release studies

All hydrogels were prepared using FITC-BSA solution (1 mg mL^{-1}) in phosphate-buffered saline (PBS) 1× as described above. Hydrogel samples were incubated in an Eppendorf tube containing 2 mL DTT solution (1 or 10 mM DTT in PBS 1×) or 2 mL GSH solution (10 μM or 10 mM GSH in PBS 1×) while shaking in a bioshaker at 37 °C for 48 hours. 1 mL aliquots were refreshed at regular time intervals (1–6th, 24th, and 48th hours) and monitored using a UV spectrophotometer. The release profiles of the hydrogel samples were determined by measuring the absorbance of FITC-BSA at 492 nm. The amount of released FITC-BSA was quantified using a standard calibration curve obtained for FITC-BSA.

Fluorescent dye conjugation and cleavage from hydrogels

One side of the swollen hydrogel sample was treated with 1 mM DTT solution for 10 min followed by washing with DI-H_2O to remove any residual reducing agent. The newly generated thiol groups were then functionalized with a 10 mM solution of 2,2′-dithiodipyridine (PDS) prepared in MeOH. After 20 min, the hydrogel sample was immersed in DI-H_2O to remove unreacted PDS and residual MeOH. A solution of the thiol-containing dye, SAMSA (1 mg mL^{-1} in DI-H_2O), was dropped onto the DTT treated side of the hydrogel and kept in the dark for 20 min to complete the thiol-exchange reaction. The hydrogel was immersed in DI-H_2O again to remove the unbound fluorescent dye. To enforce the dye release, the sample surface was treated with 1 mM DTT solution for 10 min. All four steps (DTT → PDS → SAMSA → DTT) were monitored using fluorescence microscopy. Functionalization with TAMRA-maleimide for irreversible conjugation was undertaken using the same protocol. A solution of TAMRA-maleimide (1 mg mL^{-1}) was dropped onto the free thiol-containing side of the hydrogel, followed by washing to remove the unreacted dye. All steps (DTT → TAMRA) were monitored using fluorescence microscopy.

3D printing of a disulfide-containing hydrogel

An extrusion-based 3D bioprinter equipped with a pneumatically driven print head was utilized for all printing protocols. The precursor hydrogel solution (HG-2_{50}) containing gellan gum (GG, 1.5% wt/v) was prepared as described above, then loaded into a 3 mL printing cartridge fitted with a 20-gauge needle (0.580 nm nozzle diameter) and stored at room temp-

erature for 1 hour. An extrusion pressure of 12–15 kPa with a printing speed of 1 mm s^{-1} was applied to dispense the solutions out of the nozzle onto a 25 °C print bed. UV light (365 nm, 10 mW cm^{-2}) was utilized for photo-crosslinking the printed scaffolds. The square constructs were printed according to a CAD model with dimensions of 20 × 20 × 3 mm, consisting of five layers with a first layer height of 0.58 mm.

Biological assays

L929 mouse fibroblast cells were purchased from ATCC (LGC Standards, Germany). 100 μL of cell suspensions, containing 5000 cells per well in a culture medium, were seeded into a 96-well plate and incubated at 37 °C for 24 hours for a CCK8 (Cell Counting Kit-8, Fluka) viability assay. Hydrogel samples (0.5 and 1 mg) were placed into the culture plate and incubated under 5% CO_2 at 37 °C for 24 hours, followed by two PBS washes. 10% CCK-8 solution was added to the cell-attached wells and incubated for 3 hours, after which the absorbance at 450 nm was measured using a microplate reader (Multiscan FC, Thermo Scientific, USA). The 10.6.1 version of GraphPad prism was employed to generate viability curves related to the corresponding cell counting values. Cell viability against degradation byproducts of hydrogels treated with DTT was assessed using the same protocol. Aliquots (5 and 10 μL) of degradation samples were transferred into culture plates and incubated under 5% CO_2 at 37 °C for 24 hours. For the live and dead viability assay, L929 cell suspensions (20 000 cells per well in Dulbecco's modified Eagle's (low) medium) were seeded into a 12-well plate and incubated at 37 °C for 24 hours. The hydrogel samples (1 mg) were placed into cell-attached wells and incubated at 37 °C. After 24 hours incubation, the wells were cleaned to remove hydrogel residuals by two PBS washing. Cells were treated with 10 μL of calcein-AM and 5 μL of propidium iodide (PI) (live and dead assay kit) (Sigma, 04511-1KT-F) in PBS solutions and incubated at 37 °C for 30 min. The same live and dead assay protocol was applied to cell cultures treated with 5 and 10 μL of degradation byproducts and incubated with cultured wells at 37 °C. Stained

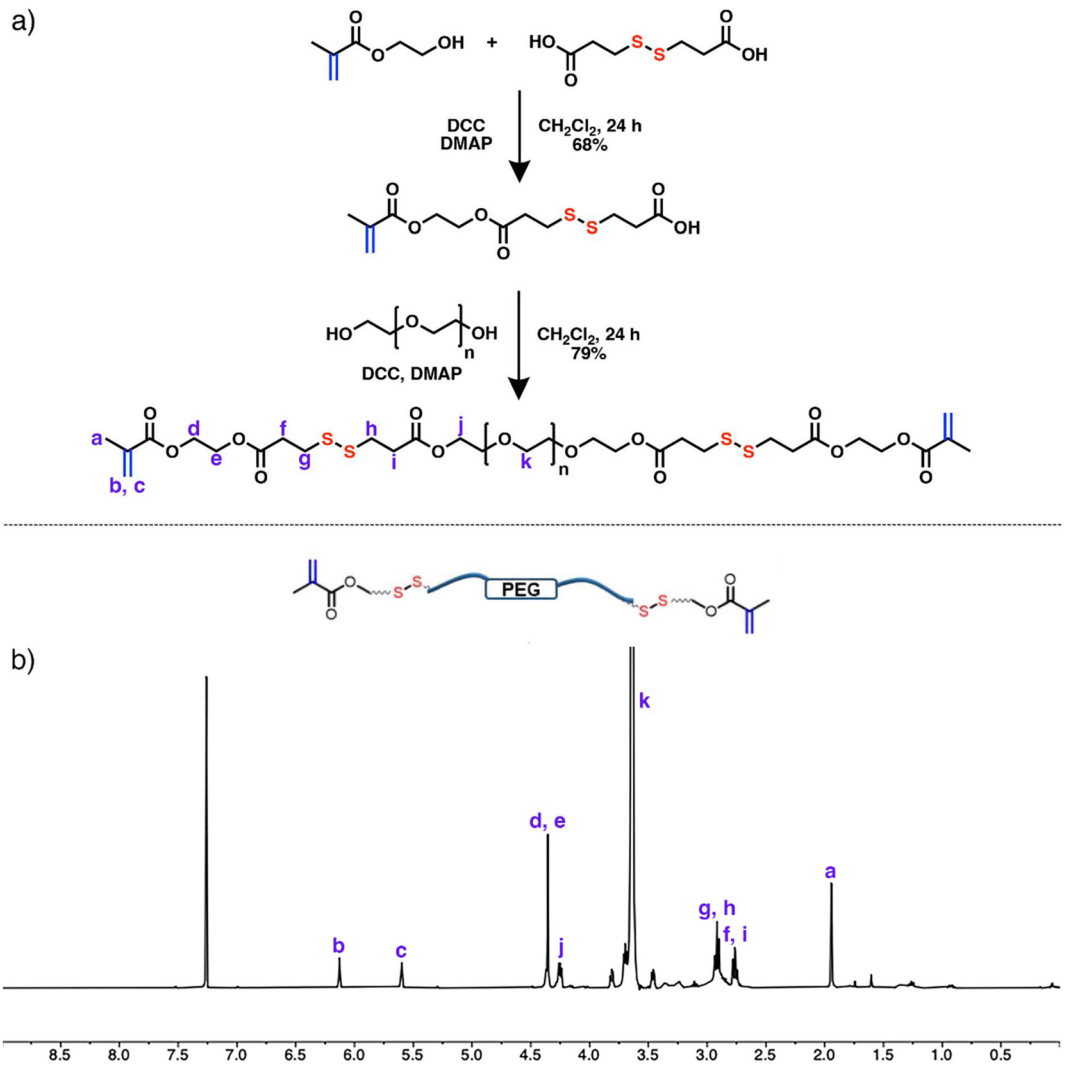

Fig. 1 (a) Synthesis of PEGDMASS using commercially available PEG polymers and (b) ^{1}H NMR spectrum of the PEGDMASS macro-crosslinker.

wells were recorded using a fluorescence microscope (Zeiss Z1 Observer inverted microscope with an AxioCam MRc5 camera). A Zeiss Filter set 38 (excitation BP: 470/40, emission BP: 525/50) was employed for visualizing green live cells attached to the wells. Zeiss Filter set 43 (excitation BP: 545/25, emission BP: 605/70) was used for imaging red dead cells in the wells.

Results and discussion

Synthesis of a disulfide-containing PEG-dimethylacrylate (PEGDMASS) crosslinker

Initially, a disulfide-containing methacrylate/carboxylic acid-terminated polymer (HEMASS) was synthesized utilizing hydroxyethyl methacrylate and 3,3′-dithiodipropionic acid in accordance with a previously reported protocol.[40] HEMASS serves as a reagent for modifying alcohol-terminated polyethylene glycol (PEG) polymers, thereby facilitating the synthesis of redox-responsive poly(ethylene glycol) dimethacrylate. Commercially available alcohol-terminated PEG was modified with HEMASS through DCC/DMAP coupling to obtain the redox-responsive macro-crosslinker PEGDMASS (Fig. 1a). The purity and chemical composition of PEGDMASS were verified utilizing ^{1}H, ^{13}C NMR and FTIR spectroscopy, and GPC. The FTIR spectrum revealed the presence of a carbonyl band at approximately 1740 cm^{-1} (Fig. S1). Additionally, the end-group functionalization of PEGDMASS was substantiated through the SEC analysis, which indicated a slight increase in the molecular weight of the polymer (Fig. S2). The number average molecular weights of the polymers were obtained using PMMA calibrants, and hence, were slightly different from the exact molecular weight provided by the supplier, but the expected shift to higher molecular weight upon functionalization was unambiguous. The molecular structure of PEGDMASS was examined using NMR spectroscopy; notably, the ^{1}H NMR spectrum of PEGDMASS confirmed the existence of proton resonances at 5.15 and 6.13 ppm, corresponding to double bond protons, and at 2.70 ppm, associated with protons adjacent to the disulfide unit (Fig. 1b). The molecular structure was also confirmed through ^{13}C NMR spectroscopy (Fig. S3).

Fabrication and characterization of hydrogels

A series of hydrogels were obtained using photopolymerization of the disulfide-containing PEG-based crosslinker, with a PEG-based methacrylate monomer, in the presence and absence of a non-degradable PEG-based crosslinker (Fig. 2). For achieving fast photopolymerization in aqueous media, LAP was used as a photo-initiator. Apart from its high solubility in aqueous media, this photo-initiator is also known to possess high compatibility with cells, because of its reduced toxicity.[41]

The dependence of the mechanical properties of PEGDMA-based hydrogels on the molecular weight and the amount of the crosslinker was investigated. To evaluate the impact of the

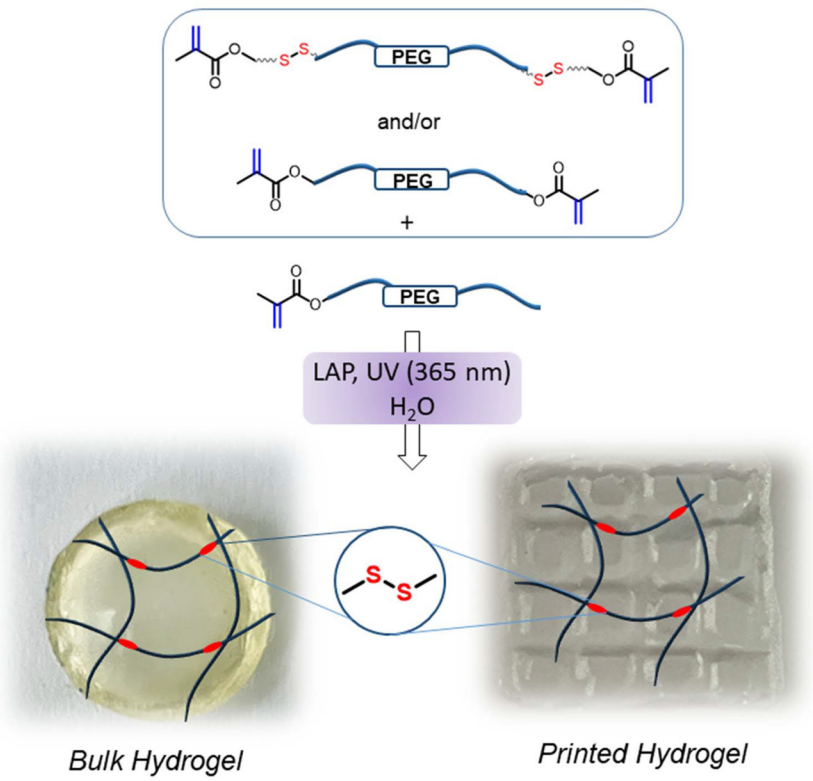

Fig. 2 Schematic illustration of the fabrication of bulk and 3D-printed hydrogels using photo-crosslinking of a mixture of crosslinkers and a PEGMEMA monomer.

molecular weight of the PEG unit on the mechanical properties of the hydrogels, firstly, PEGDMASS and PEGDMA were employed. Moreover, a range of formulations was utilized to examine the influence of varying disulfide-containing crosslinkers on the hydrogel's properties (HG-1_{100}, HG-2_{50}, HG-3_{25}, and HG-4_0). The subscripts (100, 50, 25, and 0) refer to the relative amounts of the redox-responsive PEG linker (PEGDMASS) in the hydrogels. The concentrations of PEGMEMA 5% (w/v) and LAP 0.5% (w/v) in DI-H_2O were kept constant for all hydrogels. Thus, HG-3_{25} contains one fourth amount of the redox-responsive linker compared to HG-1_{100}. In addition to the dimethacrylate crosslinkers, the hydrophilic macromonomer PEGMEMA was incorporated into all formulations to provide a spacer between the crosslinkers, as well as acting as a monomer that can be easily replaced by other functional hydrophilic monomers in future studies (Table 1).

First, HG-1_{100} and HG-4_0 were compared to evaluate the effects of the molecular weights of the crosslinkers, while HG-2_{50} and HG-3_{25} were compared to assess the impact of the overall crosslinker amount on hydrogel properties. The hydrogels were fabricated under ultraviolet light (365 nm, 10 mW cm^{-2}), resulting in disk-shaped hydrogels with a thickness of 1 mm (Fig. 3a). The swelling behavior of these hydrogels was examined using disk-shaped samples, which were incubated in PBS at 37 °C. HG-1_{100} demonstrated a swelling capacity that was more than four times greater than that of HG-4_0 (Fig. 3b), likely attributed to the higher molecular weight of PEGDMASS, which enhances network flexibility and water absorption. To investigate the impact of the PEGDMASS amount on swelling, HG-2_{50} and HG-3_{25} were compared. HG-3_{25} absorbed approximately three times more water than HG-2_{50}, suggesting that swelling can be modulated by adjusting the PEGDMASS content (Fig. 3c). Furthermore, the stability of disulfide bonds within PEGDMASS during ultraviolet crosslinking is critical for preserving the integrity of the crosslinked network. Ellman's assay was used to confirm the absence of free thiols in the fabricated hydrogels, suggesting that the exposure to ultraviolet irradiation employed during fabrication did not cleave the disulfide bonds present in the hydrogels (Fig. S4).

Given that the swelling behavior of hydrogels is intricately associated with their porosity, a comparative analysis of the surface morphology of these hydrogels was conducted. Hydrogels HG-4_0 and HG-1_{100} in their swollen state were subjected to freeze-drying for subsequent analysis. Morphological analysis of the lyophilized HG-4_0 using SEM revealed a smooth, non-porous structure; conversely, HG-1_{100} displayed a highly porous morphology, attributed to its high molecular weight crosslinker (Fig. 4). Similarly, SEM images illustrated that both HG-2_{50} and HG-3_{25} exhibited porous structures, which can be attributed to the presence of the PEGDMASS macro-crosslinker.

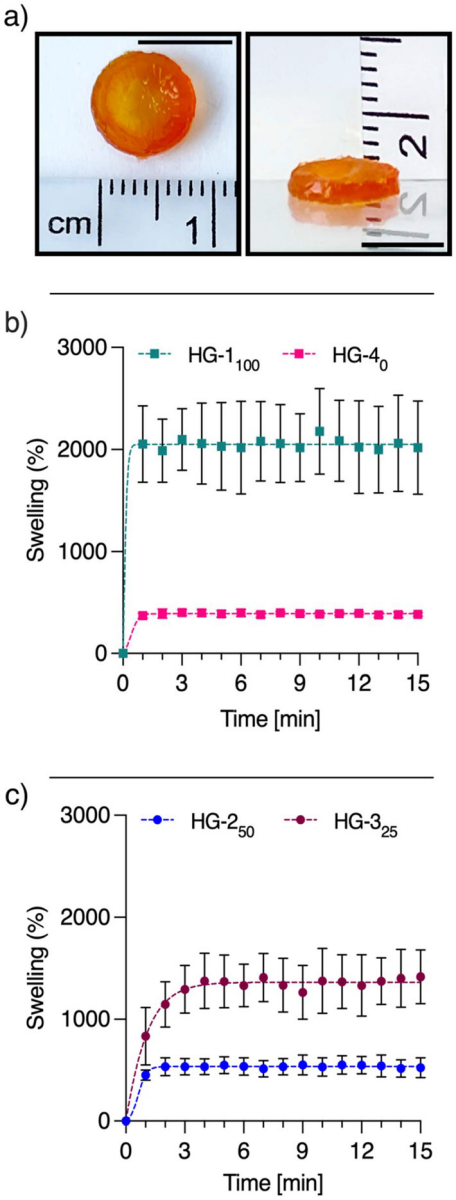

Fig. 3 (a) Representative images of a hydrogel disk. Orange food color has been added to aid visualization, (b) swelling behavior of HG-1_{100} and HG-4_0, and (c) swelling behavior of HG-2_{50} and HG-3_{25}. Scale bars in the digital images represent 1 cm.

Table 1 Composition of HGs with various amounts of degradable and non-degradable crosslinkers

Hydrogel[a]	PEGDMASS (wt/v, %)	PEGMEMA (wt/v, %)	PEGDMA (wt/v, %)	LAP (wt/v, %)
HG-1_{100}	20	5	0	0.5
HG-2_{50}	10	5	5	0.5
HG-3_{25}	5	5	5	0.5
HG-4_0	0	5	20	0.5

[a] All hydrogels were prepared using DI-H_2O containing LAP as a photoinitiator.

Redox-responsive degradation of hydrogels

The rheological properties of swollen hydrogels were further analyzed to evaluate their behavior in aqueous environments. While

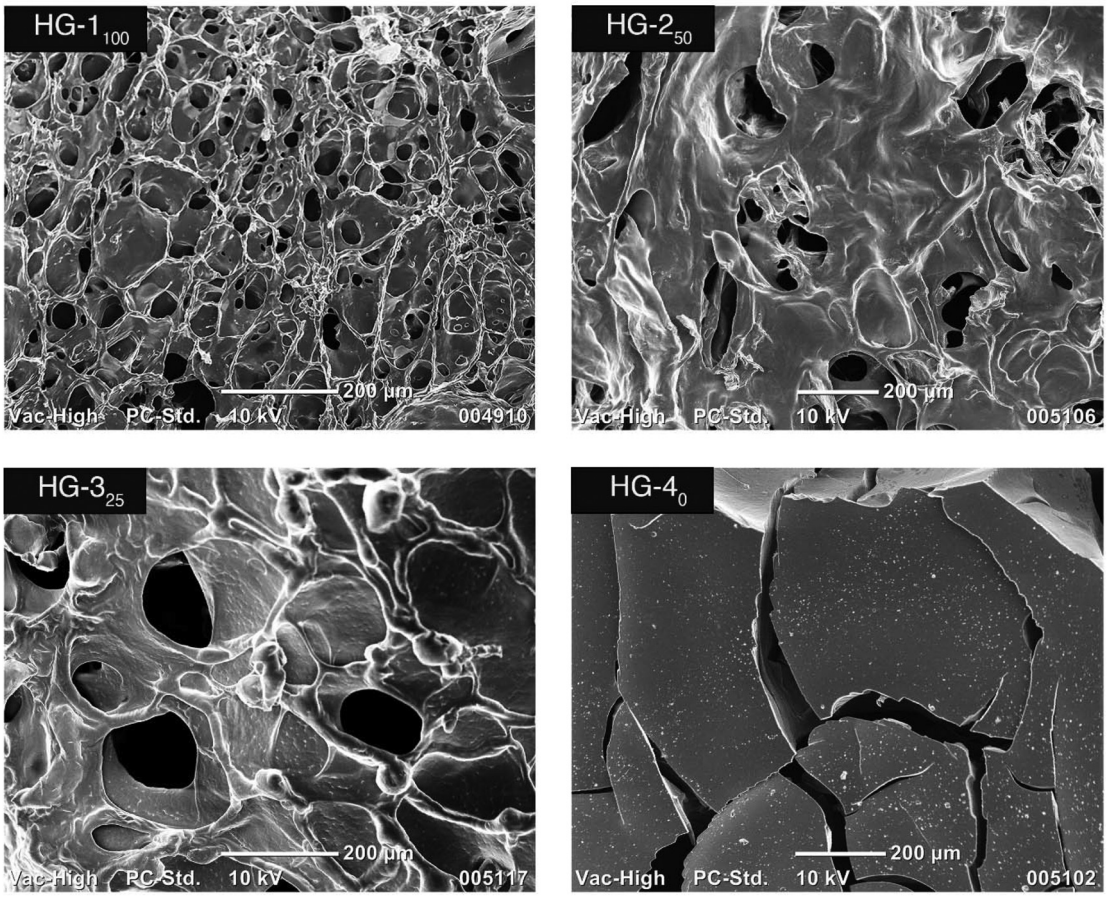

Fig. 4 SEM images of the surface morphologies of freeze-dried hydrogels.

the storage and loss moduli of HG-1_{100}/HG-4_0 and HG-2_{50}/HG-3_{25} were comparable immediately following crosslinking, they exhibited notable differences in their swollen states. These distinctions stemmed from variations in swelling behavior attributable to differences in molecular weight and concentration, which consequently impacted the mechanical properties. The amplitude sweep test demonstrated a more pronounced disparity in the storage modulus between HG-1_{100} and HG-4_0. Hydrogels incorporating PEGDMASS (HG-1_{100}, HG-2_{50}, and HG-3_{25}) exhibited an elastic-dominant behavior within the linear viscoelastic region (LVR). Conversely, HG-4_0 displayed LVR behavior only up to 2% strain, after which a marked decline occurred, indicating increased brittleness attributed to a highly dense network formed by a lower molecular weight PEGDMA crosslinker (Fig. S5). The frequency sweep tests further corroborated these observations, revealing that HG-4_0 possessed a significantly higher storage modulus than HG-1_{100}, in accordance with its lower swelling ratio (Fig. 5a). Likewise, HG-2_{50} exhibited a higher modulus than HG-3_{25}, underscoring the impact of the crosslinker amount on hydrogel stiffness. The stability of PEGDMA hydrogels is primarily governed by the stability of ester bonds within the methacrylate units in their chemical structure. Conversely, the stability of hydrogels derived from PEGDMASS is contingent upon the integrity of disulfide bonds. To assess hydrogel stability under various conditions, time sweep rheometer tests were performed on swollen HG-1_{100} in PBS and a 10 mM DTT solution at 37 °C (Fig. 5b). HG-1_{100} exhibited a stable storage modulus in PBS for two hours, signifying effective crosslinking and retention of structural integrity. In contrast, exposure to DTT (10 mM) significantly reduced the modulus, thereby confirming the redox-responsive cleavage of disulfide bonds (Fig. 5b). However, the disulfide-bond-deficient HG-4_0 maintained stability in the reducing agent (10 mM DTT), in contrast to HG-1_{100}. Visual representations of HG-1_{100} and HG-4_0 before and after incubation with DTT further demonstrate the degradation of hydrogels mediated by PEGDMASS (Fig. 5c and d).

The on-demand degradation of hydrogels can be utilized to facilitate the controlled delivery of large biomolecules, such as proteins. To investigate this, we examined the release of the fluorescently labeled protein FITC-BSA. Firstly, the release of FITC-BSA from HG-1_{100} was evaluated in the presence of 1 mM DTT and PBS at 37 °C (Fig. 6a). A lower concentration of DTT was selected to obtain a slow degradation profile for HG-1_{100}, which resulted in complete dissolution of the hydrogel within 48 hours. A significantly enhanced release was observed under a reducing environment, when compared to that under neutral conditions. For comparative analysis of the release behavior of hydrogels, all hydrogels loaded with FITC-BSA were incubated

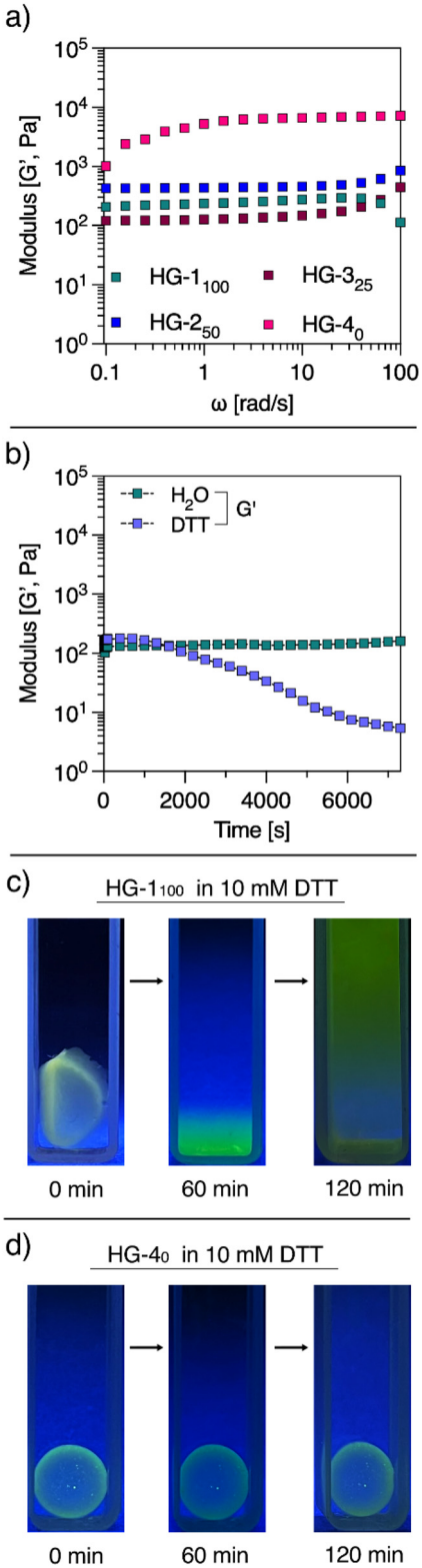

Fig. 5 (a) Angular frequency (ω) sweep test of hydrogels, (b) change in the storage modulus (G') of HG-1_{100} incubated in PBS and DTT (10 mM) at 37 °C, and (c) images of FITC-BSA containing HG-1_{100} and (d) HG-4_0 incubated in DTT (10 mM) for 120 minutes under UV light.

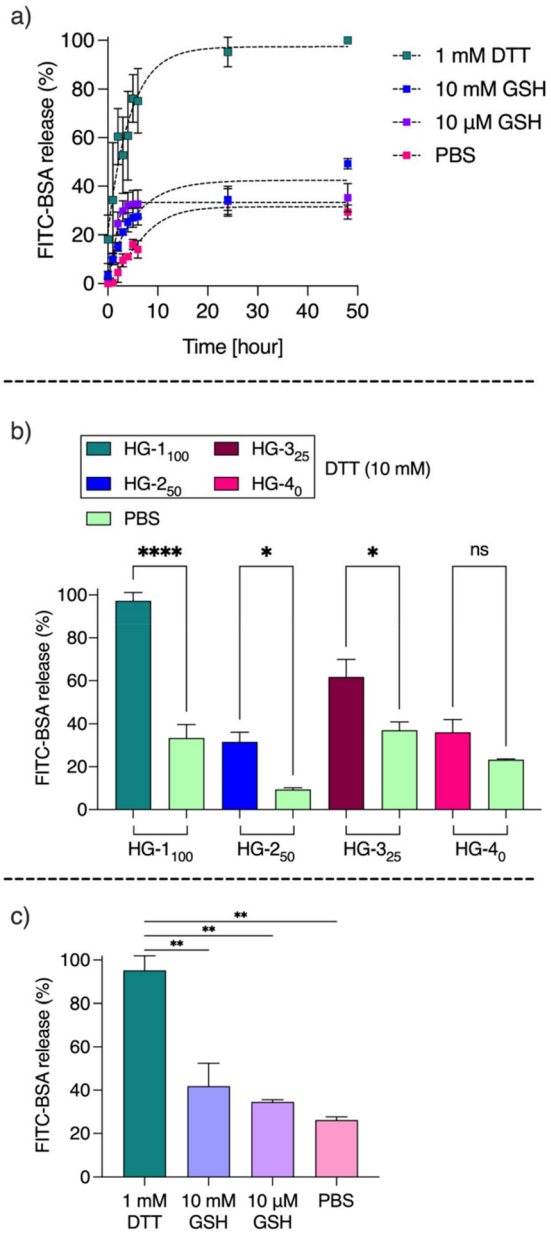

Fig. 6 FITC-BSA release profiles of hydrogels: (a) HG-1_{100} in 1 mM DTT, 10 μm GSH, 10 mm GSH, and PBS at 37 °C after 48 h, (b) the comparison between passive (in PBS) and active (in 10 mM DTT) FITC-BSA release from various hydrogels at 37 °C after 48 h, and (c) the comparison between passive (in PBS) and active (in 1 mM DTT, 10 μM GSH, and 10 mM GSH) FITC-BSA release from HG-1_{100} at 37 °C after 48 h.

in either PBS or 10 mM DTT solution at 37 °C. Despite differences in swelling and stiffness, HG-1_{100} and HG-4_0 displayed similar FITC-BSA release profiles in PBS (Fig. 6b). This suggests that the release of large molecules from a PEG-based network primarily depends on network degradation. We analyzed the release of FITC-BSA in a 10 mM DTT solution to evaluate this hypothesis. While HG-4_0 exhibited a release pattern comparable to that observed in PBS, HG-1_{100} demonstrated a significantly higher release than HG-4_0 (Fig. 6b).

Additionally, we compared FITC-BSA release from HG-2_{50} and HG-3_{25} in PBS. Despite HG-3_{25} being more porous and softer than HG-2_{50}, its release was only marginally higher in PBS. However, in the presence of DTT, HG-3_{25} exhibited a significantly enhanced release compared to HG-2_{50}, suggesting that accelerated degradation in reducing media facilitated the release of the protein. The on-demand release of FITC-BSA from HG-1_{100} was also evaluated under different reductive environments by mimicking intracellular and extracellular conditions using GSH. In Fig. 6a, the passive release behavior of protein from HG-1_{100} was examined in PBS for 48 hours at 37 °C, resulting in a 27.2% release. The extracellular conditions were mimicked using 10 μM GSH, where HG-1_{100} exhibited a 35.2% release after 48 hours at 37 °C (Fig. 6a). A notable difference was observed under intracellular conditions (10 mM GSH), where HG-1_{100} showed a higher release of FITC-BSA, reaching 49.3% (Fig. 6a). The comparative data (Fig. 6c) represent the on-demand release patterns of HG-1_{100} under different reductive environments (DTT and GSH). It should be noted that bulk hydrogels cannot be internalized by cells, but one can envision that similar GSH concentrations can be externally supplied when used as an implanted device.

Post-gelation functionalization of hydrogels

A notable characteristic of PEGDMASS-based hydrogels is their amenability for chemical functionalization. Although direct modification of these hydrogels is not feasible due to the absence of reactive handles, the partial cleavage of disulfide bonds results in the generation of highly reactive thiol groups. In this regard, the hydrogel HG-3_{25} was subjected to a brief treatment with a low-concentration DTT (1 mM) solution to generate thiol groups (Fig. 7a). After rinsing the hydrogel with water to remove any unreacted DTT, modification using a maleimide-containing dye molecule, namely TAMRA-maleimide, was undertaken. After the removal of any unbound dye by rinsing with solvents, fluorescence microscopy confirmed successful dye conjugation due to the presence of characteristic reddish emission (Fig. 7b).

In an alternative approach, the thiol groups generated in the hydrogel were converted to a pyridyl disulfide group by treatment with pyridyldisulfide, a moiety known to undergo facile thiol-disulfide exchange reaction for conjugating thiol-containing molecules reversibly (Fig. 8a). To this end, the thiol-containing fluorescein dye SAMSA was used for investigating reversible functionalization. As expected, analysis using a fluorescence microscope revealed that the SAMSA functionalized hydrogel exhibited the characteristic green fluorescence (Fig. 8b). To further validate the reversible nature of this conjugation, the SAMSA functionalized hydrogel was treated with a DTT (1 mM) solution for 10 min. While the hydrogel did not undergo significant degradation due to the presence of a sufficient amount of the non-degradable crosslinker, fluorescence microscopy revealed a remarkable reduction of the green fluorescence, suggesting the cleavage of the dye through scission of the disulfide linkage (Fig. 8c). As mentioned above, the network robustness of HG-3_{25} played a decisive role in the

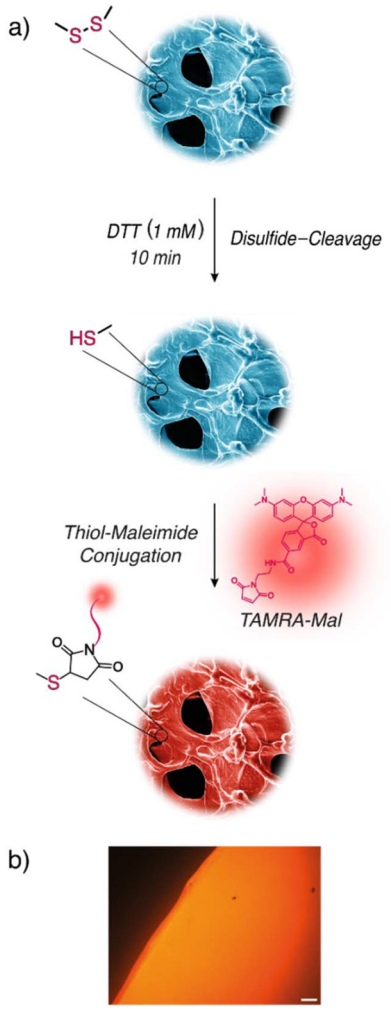

Fig. 7 (a) Schematic illustration and (b) fluorescence microscopy image of HG-3_{25} modified with a thiol-reactive maleimide-containing TAMRA dye. Scale bar in the fluorescence microscopy image is 100 μm.

functionalization of dye molecules *via* thiol-disulfide exchange and thiol-Michael addition. The comparative frequency sweep tests clearly indicated that the hydrogel remained largely intact, confirming its high mechanical integrity (Fig. S6). The fluorescent dye conjugation *via* thiol-disulfide exchange and thiol-Michael addition was further evaluated using HG-4_0. Since HG-4_0 was fabricated using PEGDMA, it served as a disulfide-bond-deficient control hydrogel. The same functionalization procedures were applied to HG-4_0, and no fluorescence was observed upon analysis with fluorescence microscopy (Fig. S7 and S8), indicating that the presence of disulfide bonds directly contributes to the functionalization observed in the hydrogel HG-3_{25}.

Biocompatibility of hydrogels

To evaluate the suitability of PEGDMASS-based hydrogels for biomedical applications, a series of cytotoxicity experiments was conducted. The cytotoxicity of HG-1_{100} on L929 cells was systematically assessed by treating pre-seeded cells in 96-well

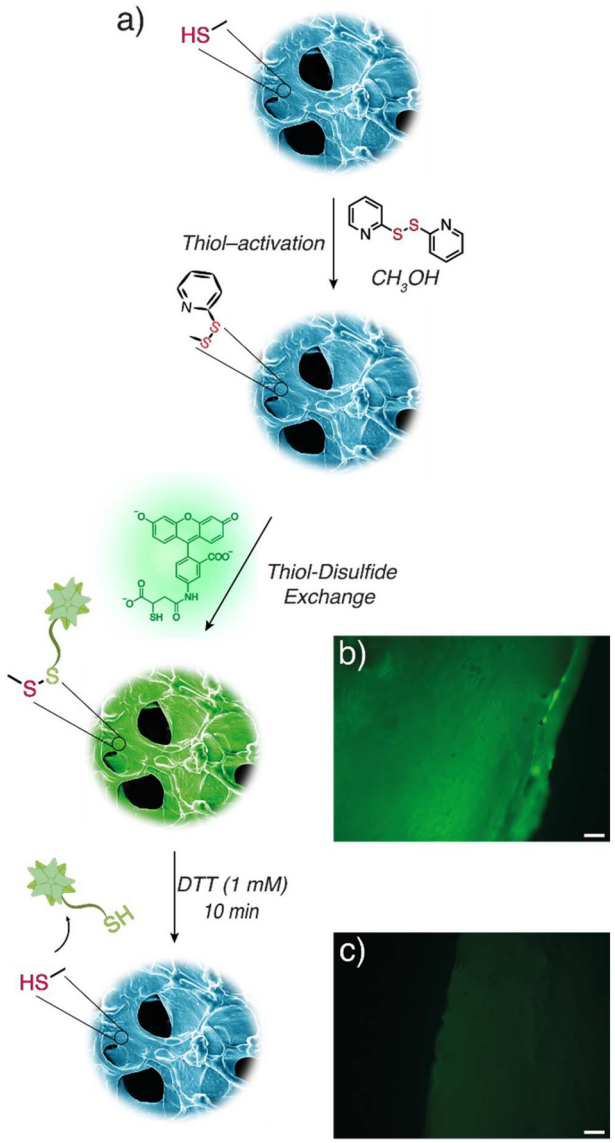

Fig. 8 (a) Schematic illustration of the activation of hydrogels with pyridyl-disulfide functional groups and their use for reversible conjugation of the thiol-containing fluorescent dye SAMSA; and fluorescence microscopy images of (b) HG-3_{25} modified with the thiol-containing SAMSA dye and (c) treated with DTT (1 mM) to cleave the attached dye. Scale bars in fluorescence microscopy images are 100 μm.

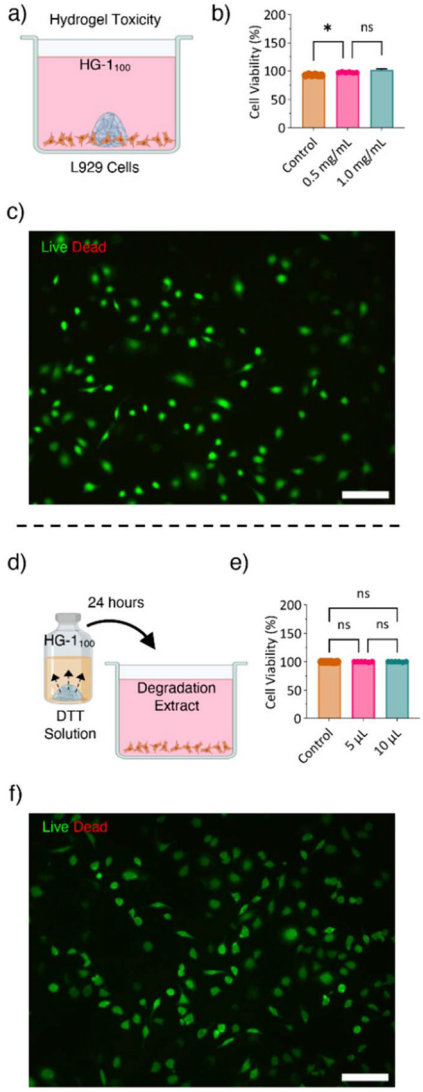

Fig. 9 (a) Schematic illustration of L929 cells treated with HG-1_{100} for 24 hours, (b) cell viability of L929 cells incubated with various concentrations of HG-1_{100}, (c) representative fluorescence microscopy image from the live/dead assay of L929 cells treated with 0.5 and 1.0 mg mL^{-1} of HG-1_{100}, (d) schematic illustration of L929 cell treatment with the degradation products of HG-1_{100}, (e) L929 cell viability following treatment with HG-1_{100} degradation products, and (f) representative fluorescence microscopy image from the live–dead assay of L929 cells treated with HG-1_{100} degradation products. Scale bars in fluorescence microscopy images are 100 μm.

plates with HG-1_{100} (1 mg) for 24 hours (Fig. 9a). The quantitative analysis indicated that cell viability in the HG-1_{100}-treated group was similar to that in the control group (Fig. 9b). A live/dead assay further corroborated the observation of minimal cell mortality following exposure to HG-1_{100} (Fig. 9c). In addition to the hydrogel HG-1_{100} itself, its degradation byproducts were also evaluated for cytotoxicity. HG-1_{100} was degraded under reducing conditions, after which L929 cells were exposed to the resultant degradation extracts (Fig. 9d). Both fluorescence microscopy and live/dead assay suggested that the degradation products were also non-cytotoxic (Fig. 9e and f).

Printing of degradable hydrogels

For extrusion-based hydrogel printing, factors such as shape fidelity of printed constructs, self-supporting ability, adjustable viscosity, and appropriate external pressure are essential for printability.[42,43] To trigger fluid flow through the nozzle, the applied pressure must exceed the yield stress,[44] which serves as a threshold of elastic behavior. Another important parameter, the flow point,[45,46] indicates the crossover point where the elastic (G') modulus equals the loss (G'') modulus. Therefore, gellan gum (GG) was incorporated into the hydrogel

precursor solution as a natural viscosity modifier to enhance its printability.[47–51] Elastic and loss moduli of HGs without GG indicated rigid behavior in the LVE region; however, yield and flow points of HGs with GG indicated improved flow, which was confirmed by comparative strain sweep tests (Fig. S9). At low shear stress, the gel-like behavior dominated over the fluid-like response. As shear stress increased, G' showed a decreasing trend, indicating the extrudability of the HGs, since fluid-like behavior becomes dominant when $G'' > G'$ under sufficient pressure.

Hydrogel precursor solutions (HG-1_{100}, HG-2_{50}, and HG-3_{25}) containing GG (1.5% wt/v) were evaluated as printable bioinks. Although all hydrogel precursor bioink formulations were printed evenly, HG-1_{100} could not retain its printed pattern, indicating poor shape fidelity, and HG-3_{25} did not have adequate mechanical strength to support a free-standing construct due to a smaller amount of crosslinker. Therefore, HG-2_{50} was determined to be a suitable bioink formulation for a free-standing printable hydrogel. The GG-containing HG-2_{50} hydrogel ink was continuously extruded to form a high-resolution 3D construct with a customized grid pattern with 18% infill density that was designed in CAD software. The printed hydrogels were photo-crosslinked under UV light (365 nm, 10 mW cm^{-2}) at room temperature to obtain printed scaffolds that could be lifted off from the glass substrate (Fig. 10a). As a further proof of concept of on-demand degradability, the disulfide bonds in the 3D-printed construct were reduced under reducing conditions (100 mM DTT) (Fig. 10b). Upon incubation in a reducing environment, the printed scaffolds rapidly disintegrated (Fig. 10c and Fig. S10).

The mechanical integrity of 3D-printed scaffolds was assessed following post-printing stability tests. To this end, long-term structural integrity was evaluated in DI-H_2O. The 3D-printed hydrogels were immersed in DI-H_2O for up to 7 days. Stability was examined by measuring the mass (%) of each scaffold after predetermined immersion periods. Representative mass values recorded over a 7 day period showed a negligible mass loss (0.2%) (Fig. S11). The findings indicated that the printed scaffolds exhibit high stability and remain intact over prolonged periods under neutral conditions, while degrading in reducing environments.

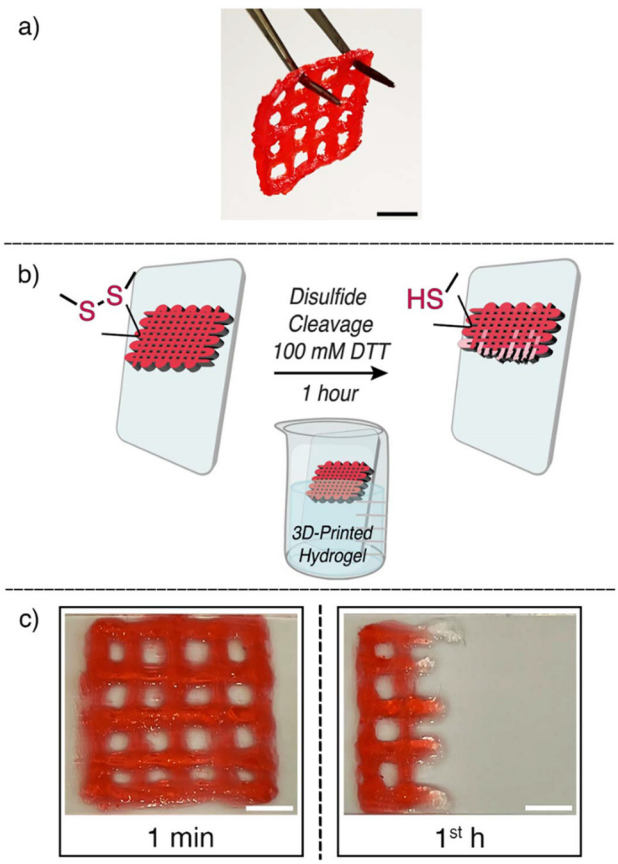

Fig. 10 (a) 3D-printed disulfide-containing hydrogel (HG-2_{50} ink based) (scale bar is 500 μm), (b) schematic illustration of the 3D-printed hydrogel under reducing conditions, and (c) images of the disulfide-containing 3D-printed hydrogels before and after treatment with a reducing solution (100 mM DTT in PBS, room temperature) (scale bar is 500 μm).

Conclusions

In this study, we successfully synthesized a redox-responsive PEG-dimethacrylate crosslinker and demonstrated its utility in modulating the mechanical and degradation properties of hydrogels. The incorporation of a disulfide-containing crosslinker enabled the formation of redox-responsive hydrogels with tunable swelling behavior, mechanical properties, and degradation kinetics. On-demand release of protein from these hydrogels was also demonstrated under reducing conditions. Moreover, partial degradation of disulfide linkers furnishes thiol-containing reactive hydrogels, which can undergo reversible and non-reversible conjugation using thiol-disulfide and thiol-maleimide chemistry, respectively. Overall, these findings highlight the potential of the disulfide-containing crosslinker disclosed here in engineering stimuli-responsive hydrogels which can find applications in biomedical sciences.

Author contributions

M. A., A. G. and S. K. performed the experiments. I. A., R. S. and A. S. provided conceptualization and supervision, and undertook the writing of the final draft. The manuscript was written through the contributions of all authors. All authors have approved the final version of the manuscript.

Conflicts of interest

The authors declare no competing financial interest.

Data availability

The data supporting this article have been included as part of the supplementary information (SI). Supplementary information: Fig. S1–S10 and Table S1 include NMR spectra, rheology data and control experiment data. See DOI: https://doi.org/10.1039/d6lp00058d.

Acknowledgements

A. G. acknowledges the financial support from the Scientific and Technological Research Council of Türkiye (TÜBITAK) through the 2210-A fellowship. The authors acknowledge the Bogazici University Center of Targeted Therapy Technologies for access to instrumentation facilities.

References

1 R. Ravichandran, S. Sundarrajan, J. R. Venugopal, S. Mukherjee and S. Ramakrishna, *Macromol. Biosci.*, 2012, **12**, 286–311.
2 B. D. Ulery, L. S. Nair and C. T. Laurencin, *J. Polym. Sci., Part B:Polym. Phys.*, 2011, **49**, 832–864.
3 D. S. Kohane and R. Langer, *Pediatr. Res.*, 2008, **63**, 487–491.
4 A. Degirmenci, R. Sanyal and A. Sanyal, *RSC Appl. Polym.*, 2024, **2**, 976–995.
5 C. L. Zaccaria, V. Cedrati, A. Nitti, E. Chiesa, A. de Ilarduya, M. Garcia-Alvarez, M. Meli, G. Colombo and D. Pasini, *Polym. Chem.*, 2021, **12**, 3784–3793.
6 H. Murata, B.-J. Chang, O. Prucker, M. Dahm and J. Rühe, *Surf. Sci.*, 2004, **570**, 111–118.
7 S. Nambiar and J. T. W. Yeow, *Biosens. Bioelectron.*, 2011, **26**, 1825–1832.
8 B. Adhikari and S. Majumdar, *Prog. Polym. Sci.*, 2004, **29**, 699–766.
9 W.-K. Oh, O. S. Kwon and J. Jang, *Polym. Rev.*, 2013, **53**, 407–442.
10 A. Degirmenci, R. Sanyal, M. Arslan and A. Sanyal, *Polym. Chem.*, 2022, **13**, 2595–2607.
11 A. Degirmenci, R. Sanyal, H.-A. Klok and A. Sanyal, *J. Am. Chem. Soc.*, 2025, **147**, 24672–24683.
12 P. Zhou, Z. Zhang, F. Mo and Y. Wang, *Adv. Sens. Res.*, 2024, **3**, 2300021.
13 K. Y. Lee and D. J. Mooney, *Chem. Rev.*, 2001, **101**, 1869–1880.
14 B. V. Slaughter, S. S. Khurshid, O. Z. Fisher, A. Khademhosseini and N. A. Peppas, *Adv. Mater.*, 2009, **21**, 3307–3329.
15 O. Erol, A. Pantula, W. Liu and D. H. Gracias, *Adv. Mater. Technol.*, 2019, **4**, 1900043.
16 R. V. Ulijn, N. Bibi, V. Jayawarna, P. D. Thornton, S. J. Todd, R. J. Mart, A. M. Smith and J. E. Gough, *Mater. Today*, 2007, **10**, 40–48.
17 Y. S. Zhang and A. Khademhosseini, *Science*, 2017, **356**, eaaf3627.
18 A. S. Hoffman, *Adv. Drug Delivery Rev.*, 2012, **64**, 18–23.
19 S. Correa, A. K. Grosskopf, H. Lopez Hernandez, D. Chan, A. C. Yu, L. M. Stapleton and E. A. Appel, *Chem. Rev.*, 2021, **121**, 11385–11457.
20 I. Altinbasak, R. Sanyal and A. Sanyal, *RSC Adv.*, 2016, **6**, 74757–74764.
21 J.-H. Ryu, S. Jiwpanich, R. Chacko, S. Bickerton and S. Thayumanavan, *J. Am. Chem. Soc.*, 2010, **132**, 8246–8247.
22 J.-H. Ryu, R. T. Chacko, S. Jiwpanich, S. Bickerton, R. P. Babu and S. Thayumanavan, *J. Am. Chem. Soc.*, 2010, **132**, 17227–17235.
23 A. L. Watson, C. Li, A. Sharif, E. R. Gillies and H. Tran, *RSC Appl. Polym.*, 2026, **4**, 205–210.
24 B. Klemm, M. Tavasso, I. Piergentili, M. Satijn, T. G. Brevé, P. E. Boukany and R. Eelkema, *RSC Appl. Polym.*, 2026, **4**, 328–335.
25 N. R. B. Boase, E. R. Gillies, R. Goh, R. E. Kieltyka, J. B. Matson, F. Meng, A. Sanyal and O. Sedláček, *Biomacromolecules*, 2024, **25**, 5417–5436.
26 L. Beria, T. N. Gevrek, A. Erdogan, R. Sanyal, D. Pasini and A. Sanyal, *Biomater. Sci.*, 2014, **2**, 67–75.
27 R. Kilic Boz, D. Aydin, S. Kocak, B. Golba, R. Sanyal and A. Sanyal, *Bioconjugate Chem.*, 2022, **33**, 839–847.
28 I. Altinbasak, S. Kocak, R. Sanyal and A. Sanyal, *Biomacromolecules*, 2022, **23**, 3525–3534.
29 M. Alkis, A. Barras, R. Boukherroub, S. Szunerits and A. Sanyal, *Macromol. Biosci.*, 2025, **26**, e00346.
30 S. Bera, R. Bej, P. Kanjilal, S. Sinha and S. Ghosh, *Bioconjugate Chem.*, 2024, **35**, 480–488.
31 B. Saha, S. Bhattacharyya, S. Mete, A. Mukherjee and P. De, *ACS Appl. Polym. Mater.*, 2019, **1**, 2503–2515.
32 A. Mondal, S. Das, A. Banerjee, A. Sengupta and M. R. Molla, *J. Macromol. Sci., Part A:Pure Appl. Chem.*, 2025, **62**, 212–223.
33 T. N. Gevrek, M. Cosar, D. Aydin, E. Kaga, M. Arslan, R. Sanyal and A. Sanyal, *ACS Appl. Mater. Interfaces*, 2018, **10**, 14399–14409.
34 J. A. Syrett, D. M. Haddleton, M. R. Whittaker, T. P. Davis and C. Boyer, *Chem. Commun.*, 2011, **47**, 1449–1451.
35 J. K. Oh, C. Tang, H. Gao, N. V. Tsarevsky and K. Matyjaszewski, *J. Am. Chem. Soc.*, 2006, **128**, 5578–5584.
36 C. R. Fellin and A. Nelson, *ACS Appl. Polym. Mater.*, 2022, **4**, 3054–3061.
37 Z. Wan, W. H. Lee, Y. Wang, A. Shegiwal and D. M. Haddleton, *RSC Appl. Polym.*, 2024, **2**, 415–425.
38 X. Li, R. Yu, Y. He, Y. Zhang, X. Yang, X. Zhao and W. Huang, *ACS Macro Lett.*, 2019, **8**, 1511–1516.
39 G. N. Kamble and A. Sk, *ACS Appl. Polym. Mater.*, 2025, **7**, 1401–1410.
40 P. Laskar, J. Dey and S. K. Ghosh, *J. Colloid Interface Sci.*, 2017, **501**, 22–33.
41 H. Xu, J. Casillas, S. Krishnamoorthy and C. Xu, *Biomed. Mater.*, 2020, **15**, 055021.
42 S. Kyle, Z. M. Jessop, A. Al-Sabah and I. S. Whitaker, *Adv. Healthcare Mater.*, 2017, **6**, 1700264.

43 S. C. Lee, G. Gillispie, P. Prim and S. J. Lee, *Chem. Rev.*, 2020, **120**, 10834–10886.
44 P. A. Amorim, M. A. d'Ávila, R. Anand, P. Moldenaers, P. Van Puyvelde and V. Bloemen, *Bioprinting*, 2021, **22**, e00129.
45 M. I. Calafel, M. Criado-Gonzalez, R. Aguirresarobe, M. Fernández and C. Mijangos, *Mater. Adv.*, 2025, **6**, 4566–4597.
46 Z. Jiang, B. Diggle, M. L. Tan, J. Viktorova, C. W. Bennett and L. A. Connal, *Adv. Sci.*, 2020, **7**, 2001379.
47 T. Jungst, W. Smolan, K. Schacht, T. Scheibel and J. Groll, *Chem. Rev.*, 2016, **116**, 1496–1539.
48 A. I. Cernencu and M. Ioniță, *Carbohydr. Polym.*, 2023, **309**, 120676.
49 L. R. Stevens, K. J. Gilmore, G. G. Wallace and M. in het Panhuis, *Biomater. Sci.*, 2016, **4**, 1276–1290.
50 S. Wu, R. Xiao, Y. Wu and L. Xu, *Carbohydr. Polym.*, 2024, **324**, 121484.
51 J. Radhakrishnan, A. Subramanian, U. M. Krishnan and S. Sethuraman, *Biomacromolecules*, 2017, **18**, 1–26.